Integrated Electromagnetic Second Stage Microactuator for a Hard Disk Recording Head

Dragan Dinulovic[1], Henry Saalfeld[1], Zbigniew Celinski[2], Stuart B. Field[3], and Hans H. Gatzen[1]

[1]Center for Production Technology, Institute for Microtechnology, Leibniz Universitaet Hannover, 30823 Garbsen, Germany
[2] Center for Magnetism and Magnetic Nanostructures, University of Colorado, Colorado Springs, CO 80918 USA
[3]Department of Physics, Colorado State University, Fort Collins, CO 80523 USA

A slider with an integrated microactuator (SLIM) allows actuating a read-write element of a hard disk drive (HDD) in both the vertical direction allowing a flying height adjustment as well as in the lateral direction allowing a second stage actuation. The microactuator system consists of a pair of electromagnetic variable reluctance (VR) micro actuators. The microactuator system is fabricated using thin-film technology. Each actuator has a permalloy C-core carrying a two-layer spiral Cu coil with a total of 16 turns. The insulation materials are SU-8 (in the lateral direction) and Si_3N_4 (in the vertical direction). The total size of one magnetic VR microactuator is 460 μm × 300 μm × 61 μm. This paper discusses design considerations, presents the FEM simulation conducted, describes the fabrication technology, and provides experimental results.

Index Terms—**Electromagnetic microactuator, flying height adjustment, second stage actuation.**

I. Introduction

For advanced hard disk drive (HDD) recording heads, both a flying height adjustment and a second stage track-following capability for fine tracking is desirable [1]–[3]. To fulfill these requirements in a cost competitive way, a slider with an integrated microactuator (SLIM) was proposed [4]. Fig. 1 presents a schematic representation of the SLIM design. The dimensions of the SLIM correspond to a pico-slider (1.240 μm × 990 μm × 300 μm). SLIM allows for both vertical (for head-to-disk spacing adjustment) and lateral (for fine tracking) motion of the read–write element. To do so, the complete integrated microactuator system contains a pair of variable reluctance (VR) microactuators. They activate a mounting block to which a chiplet containing the read–write element is attached. The actuator is capable of moving the read–write element on the chiplet both in the vertical direction (adjusting the flying height) and in the lateral direction (allowing second stage actuation). This paper describes the design and fabrication of the electromagnetic microactuator used for SLIM. The system integration, mounting of the magnetic and mechanical parts, and experiments on a scaled-up model are described in [4].

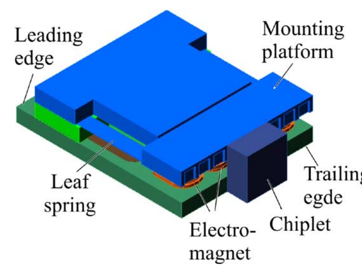

Fig. 1. Schematic representation of a SLIM.

II. Magnetic Core Properties

For accurately simulating a magnetic microdevice, the magnetic material properties of the microcomponents have to be known. As a soft magnetic material for the magnetic actuator, the permalloy NiFe45/55 was chosen since previous investigations proved the material's suitability for actuator applications [5], [6]. The most essential parameter is the relative permeability μ_r, which influences the system's reluctance. The relative permeability μ_r in thin films not only depends on the thickness of the magnetic film: for micro electromechanical system (MEMS) components, it is also strongly influenced by the structure's shape. Vibrating sample magnetometer (VSM) measurements with arrays of the desired magnetic structures allow an estimate of the relative permeability μ_r reached by a component [7].

Based on the results, for a magnetic film thickness of 20 μm, a relative permeability μ_r of 200 was assumed. In order to minimize the actuator's height, simulations were performed based on magnetic flux closure thicknesses of 5, 10, and 20 μm. The relative permeabilities μ_r chosen were 600, 450, and 200, respectively.

III. Microactuator Design

For establishing the SLIM electromagnets, a finite element method (FEM) analysis was performed using the software tool ANSYS Multiphysics. 2-D and 3-D simulations were executed to determine the optimal dimensions of the magnetic core.

To find an optimum between design and technology issues, the technological aspects of the thin-film fabrication also have to be taken into account during the simulations. Important parameters for the fabrication are aspect ratio and flank angle, defined by the photolithography processes employed. Therefore, during the modeling of the microdevices, the lateral geometry features of the fabricated structure were considered in the design process and simulation.

Based on the FEM results, the features and dimensions for the microactuator were finalized. Each magnetic microactuator

Digital Object Identifier 10.1109/TMAG.2008.2002600

Color versions of one or more of the figures in this paper are available online at http://ieeexplore.ieee.org.

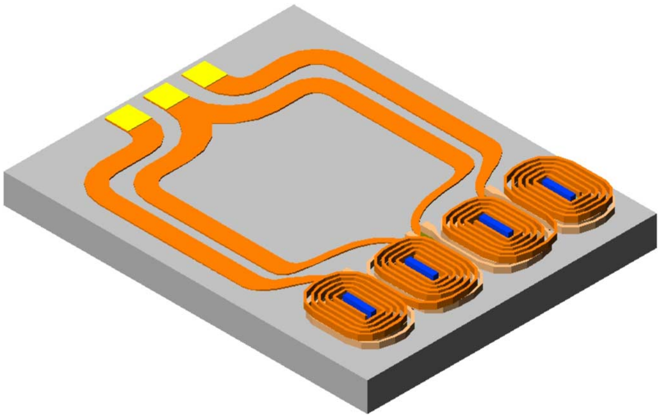

Fig. 2. Schematic view of the magnetic actuator chip.

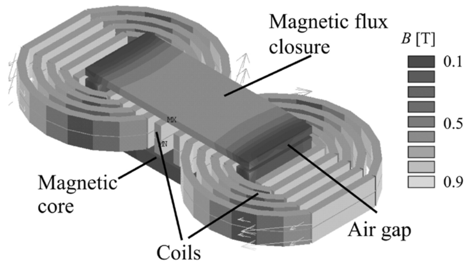

Fig. 3. Three-dimensional simulation of the magnetic flux density of the microactuator with a 10 μm flux closure.

consists of a U-shaped soft magnetic core and two double layered spiral coils for the excitation. The total size of one magnetic actuator is 438 μm $\times$ 282 μm $\times$ 61 μm. Each pole carries a two-layer coil, and the total number of turns of a VR microactuator is 20. Two VR micro actuators are integrated in the slider (Fig. 2). The mounting platform is suspended on leaf springs and contains magnetic elements which provide a flux closure. This allows both a vertical and rotational motion of the chiplet (with the read–write element on it) attached to the mounting platform. A detailed description of the fabrication and assembly process of the system is presented in [4].

For the chosen actuator design (magnetic core thickness of 20 μm and flux closure thickness of 10 μm) both 2-D and 3-D simulations were performed. Fig. 3 shows a 3-D FEM simulation result for the magnetic flux density, an excitation current of 175 mA, and an air gap of 5 μm.

Fig. 4 shows a force characteristic of the microactuator for different exciting currents and air gaps. A 2-D simulation predicted a magnetic force of about 355 μN at an air gap of 2.5 μm while exciting the coils with a current of 175 mA. A 3-D simulation resulted in very similar values: a magnetic force of about 340 μN for the same air gap.

IV. Microactuator Fabrication

The microactuator was fabricated in thin-film technology. The wafer process to fabricate the actuator mainly uses high aspect ratio microstructure technology (HARMST), combining UV depth lithography and electroplating. The materials employed were permalloy NiFe45/55 for the magnetic flux guides and magnetic poles, Cu for the coils, a photosensitive epoxy (SU-8) for lateral insulation, and low stress Si_3N_4 for insulating the two coil layers from each other [8]. As mentioned before, NiFe45/55 was chosen as the magnetic material. It has a saturation flux density B_s of 1.6 T and a high relative permeability $\mu_{r.}$ To achieve a constant magnetic layer thickness as well as flat surfaces, chemical–mechanical polishing (CMP) was applied. By using a Si_3N_4 layer deposited by plasma-enhanced chemical vapor deposition (PECVD) for the vertical insulation layers, the total height of the microactuator could be minimized. Compared to using SU-8 for the vertical insulation, Si_3N_4 allowed a reduction of the total height of the microactuator from 90 to 62 μm. Si_3N_4 deposited by PECVD also shows an excellent edge coverage, minimal tensile stress, and a good transfer of the Joule's heat created in the coil.

Fig. 5 depicts a schematic representation of the processing steps of the microactuator. For fabricating the microactuator, a 525-μm-thick Si wafer was used. For the application in SLIM, it ultimately requires a thinning to a height of 100 μm. To begin with, the wafer was coated with a Si_3N_4 insulation layer created by PECVD deposition. The first microactuator fabrication step was sputter depositing an Au seed layer. In four photolithography steps, as well as Ni, NiFe45/55 and Cu electroplating steps, respectively, fiducials, the flux guide, the electric leads, and vias as contacts between electric leads and future coils were fabricated. At the end of this process sequence, an ion beam etching (IBE) step removed the Au seed layer [Fig. 5(a)].

Next, the fabricated magnetic core structures are embedded in SU-8. After the embedding, a planarization step followed to achieve a constant magnetic layer thickness as well as flat surfaces. For this step, CMP was used. To open the windows for the poles, the Si_3N_4 layer was patterned. This was done by creating an etch mask using AZ photo resist, followed by an IBE step and resist stripping [Fig. 5(b)].

The next sequence of fabrication steps served for the creation of the lower coil layer. First, an Au seed layer was deposited. Next, AZ micromolds were created using photolithography, followed by an electroplating step of Cu. After completing the deposition of the first coil layer, the photoresist was stripped and the seed layer was removed by IBE.

The fabrication of magnetic poles started with the sputter deposition of a NiFe seed layer. Next, a photolithography step created an AZ photoresist mask serving as a micromold. In the following step, the magnetic poles were created by electroplating. Then, the photoresist was stripped and the NiFe seed layer was removed by IBE. To conclude this sequence, coils and magnetic poles were embedded in an SU-8 layer serving as lateral insulation. Using CMP, the magnetic poles were planarized [Fig. 5(c)]. Next, a Si_3N_4 layer was deposited. It serves as vertical insulation between coil layers [Fig. 5(d)]. This step concludes creating the bottom coil layer including the respective pole portions.

The first step for creating the upper coil layer was patterning the Si_3N_4 layer to create windows for the poles and the vias [Fig. 5(e)]. The patterning is done by a combination of photolithography and IBE. For the remaining process, the same sequence of fabrication steps was applied as for the first layer. Fig. 5(f) depicts the finished coil and pole structures and Fig. 5(g) the completed actuator micromagnetics.

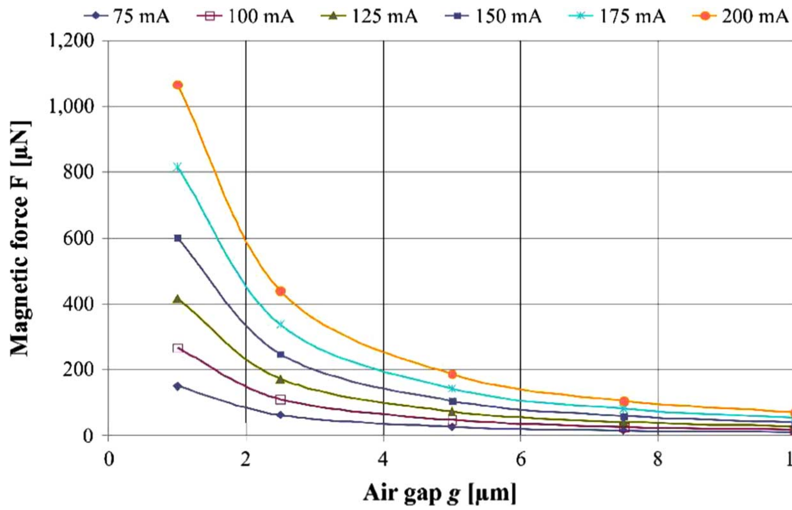

Fig. 4. Three-dimensional simulation result of the magnetic force versus actuator air gap for different exciting currents.

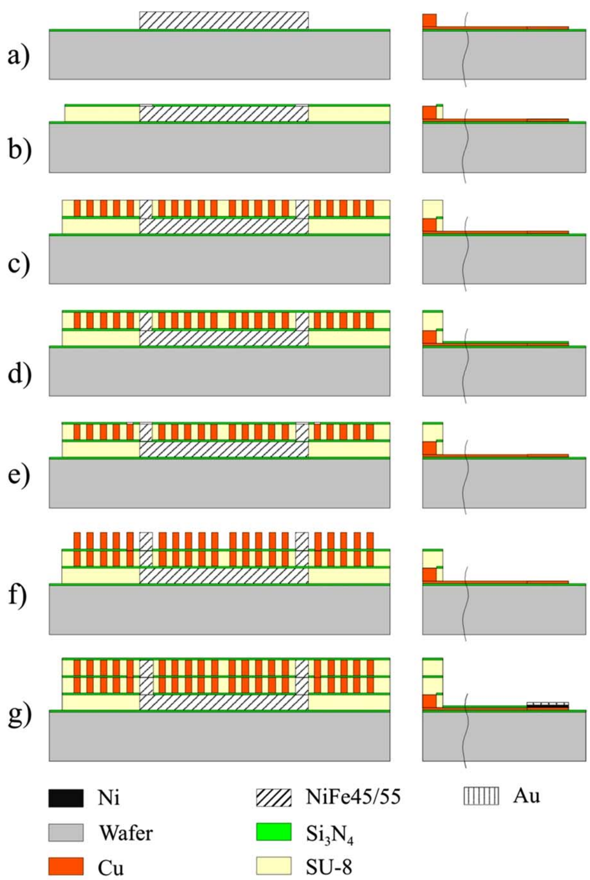

Fig. 5. Fabrication steps of the microactuator system.

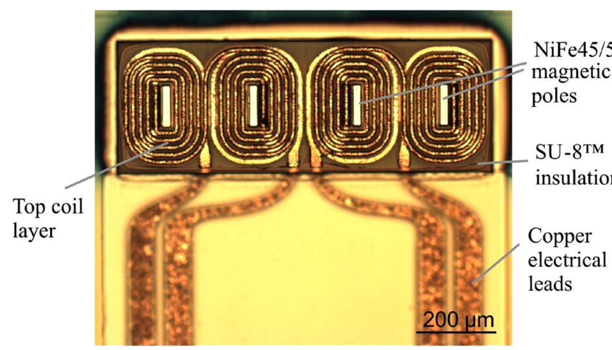

Fig. 6. Micrograph of fabricated micro actuator system.

Fig. 6 shows an optical micrograph of the microactuator system. Coils and cores are visible due to the fact that cured SU-8 is transparent.

V. Evaluation

For a functional evaluation, the LUH teamed up with the University of Colorado, Colorado Springs and Colorado State University, Fort Collins. For executing such evaluations, prototypes were subjected to force and field measurements.

Qualitative force measurements were conducted at the LUH by allowing the microactuator to exert forces on a NiFe45/55 stripe. The system was able to attract the stripe, which was a qualitative proof of its function.

For evaluating if the microactuator meets its requirements, the field created by the poles was measured. Working against air is not the regular operating mode of this device. In its actual operation, the SLIM attracts a movable flux guide located at the micromechanics. However, a field measurement is only possible if the closing flux guides are not present. This also constitutes an excitation mode not covered by the FEM simulations used to design the device. Therefore, additional FEM simulations with the flux closure removed (i.e., working against air) were necessary. They were conducted by the LUH. The field measurements were conducted at Colorado State University. To do so, the magnetic field above the pole pieces was imaged using scanning Hall probe microscopy. The Hall sensor, fabricated from a GaAs/AlGaAs hetero-structure, has an active area of approximately 1 μm^2. In the scanning configuration used, the probe was sensitive only to the z component of the magnetic field, i.e., to the component perpendicular to the scan plane. The probe had a sensitivity of 2.0 μV/G. The movement of the Hall sensor above the actuator was controlled by piezoelectric elements [9]

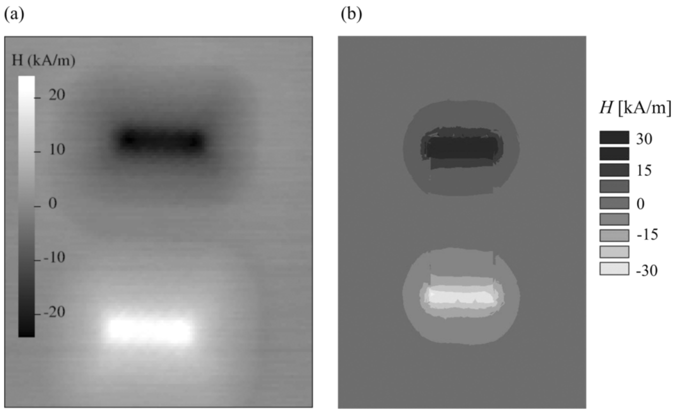

Fig. 7. Field distribution above the core. (a) Measured field strength 8 μm above the poles for an excitation current of 130 mA. (b) Simulated field strength 8 μm above the poles for an excitation current of 130 mA.

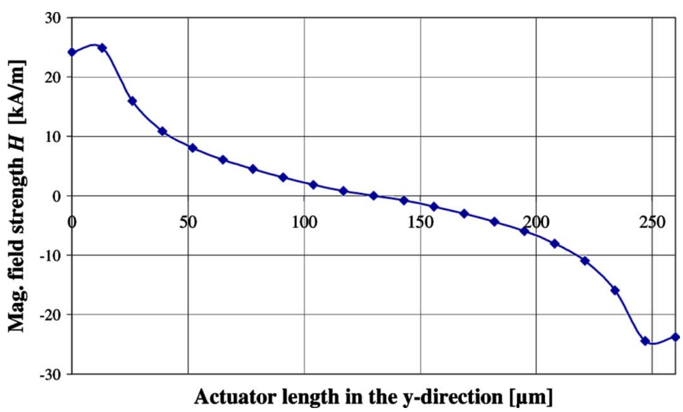

Fig. 8. FEM simulation results for the field strength along the center of the poles for the 8 μm above the poles for an excitation current of 130 mA.

and consisted of 128 steps in the x and y directions. Fig. 7(a) shows the strength of the z component of the magnetic field at a height of 8μm above an actuator's pole pieces at a coil current of 130 mA. Fig. 7(b) shows our ANSYS simulation results for this actuator at the same distance (8 μm) when current flowing through the coil is 130 mA. The difference between the measured results and simulation is in the order of 20% (simulated results are higher).

For one of the measurement conditions, an FEM simulation against air was executed. Fig. 8 shows the magnetic field strength H results across the center of the two poles at a distance of 8 μm from the pole face and for an excitation current of 130 mA. While the measurements showed a maximal magnetic field strength of 20 kA/m, the simulations predict a field strength of 25 A/m. Therefore, the measurements show an actual field strength that is 20% below the theoretical prediction. Given the challenges in determining the actual relative permeability μ_r and a measurement uncertainty of ± 3 μm for the experimental data, the results are encouraging.

VI. Conclusion

An electromagnetic microactuator system for hard disk recording heads could be developed and fabricated. For designing the microactuator system, FEM simulations were performed. One of the challenges reaching realistic FEM results is to appropriately predict the magnetic core's relative permeability μ_r. Since the energy a microactuator is capable of converting scales with its volume, a rather great building height of approximately 60 μm was chosen. By applying HARMST, such an actuator system could be fabricated. By using an organic material (SU-8) as the lateral insulation material and an inorganic material (Si_3N_4) for the vertical insulation still enabled a rather compact coil design. A comparison between field measurements conducted on the finished device and theoretical simulation data yielded encouraging results.

Acknowledgment

This work was sponsored by the European Commission within the Framework 6 Information Society Technologies Programme's Specific Target Research Project (STREP) PARMA (Performance Advances in Recording through Micro Actuation).

References

[1] J.-Y. Juang, H. Kubotera, and D. B. Bogy, "Effects of track-seeking motion on the flying attitudes of ultralow flying sliders," *IEEE Trans. Magn.*, vol. 42, no. 10, pp. 2522–2524, Oct. 2006.

[2] M. Kurita and K. Suzuki, "Flying-height adjustment technologies of magnetic head," *IEEE Trans. Microelectromech. Syst.*, vol. 40, no. 1, pp. 332–336, Feb. 2004.

[3] H. Du, G. K. Lau, and B. Liu, "Actuated suspensions with enhanced dynamics for hard disk drives," *IEEE Trans. Magn.*, vol. 41, no. 10, pp. 2887–2889, Oct. 2005.

[4] H. H. Gatzen, P. J. Freitas, E. Obermeier, and J. Robertson, "A slider with an integrated microactuator (SLIM) for second stage actuation in hard disc drives," presented at the Intermag 2008, Madrid, Spain.

[5] M. C. Wurz, D. Dinulovic, and H. H. Gatzen, "Investigations on the permeability of electroplated and sputtered permalloy," in *Proc. 8th Int. Symp. Magn. Mater., Processes Devices*, 2004, pp. 525–536.

[6] H. H. Gatzen, "Magnetic materials in thin film sensors and actuators," in *Proc. 8th Int. Symp. Magn. Mater., Processes Devices*, 2004, pp. 457–470.

[7] M. Bedenbecker, Z. Celinski, and H. H. Gatzen, "Directional permeability dependence in electroplated permalloy layers," *ECS Trans.*, vol. 3, no. 25, pp. 123–135, 2007.

[8] C. Ruffert and H. H. Gatzen, "Fabrication and test of multilayer microcoils with a high packaging density," in *HARMST 2007*, Besancon, France.

[9] J. Siegel, J. Witt, N. Venturi, and S. Field, "Compact large-range cryogenic scanner," *Rev. Sci. Instrum.*, vol. 66, pp. 2520–, 1995.

Manuscript received March 03, 2008. Current version published December 17, 2008. Corresponding author: D. Dinulovic (e-mail: dinulovic@imt.uni-hannover.de).